Difference in magnetic and ferroelectric properties between rhombohedral and hexagonal polytypes of $AgFeO_2$: A single-crystal study

Noriki Terada,[1,*] Yuta Ikedo,[2] Hirohiko Sato,[2,†] Dmitry D. Khalyavin,[3] Pascal Manuel,[3] Fabio Orlandi,[3] Yoshihiro Tsujimoto,[1] Yoshitaka Matsushita,[1] Atsushi Miyake,[4] Akira Matsuo,[4] Masashi Tokunaga,[4] and Koichi Kindo[4]

[1]*National Institute for Materials Science, Sengen 1-2-1, Tsukuba, Ibaraki 305-0047, Japan*

[2]*Department of Physics, Chuo University, 1-13-27 Kasuga, Bunkyo-ku, Tokyo 112-8551, Japan*

[3]*ISIS facility, STFC Rutherford Appleton Laboratory, Chilton, Didcot, Oxfordshire OX11 0QX, United Kingdom*

[4]*Institute for Solid State Physics, University of Tokyo, 5-1-5 Kashiwanoha, Kashiwa, Chiba 277-8581, Japan*

(Received 18 September 2018; published 1 February 2019)

We have investigated magnetic and dielectric properties of rhombohedral $3R$-$AgFeO_2$ and hexagonal 2H-$AgFeO_2$ by using magnetic and dielectric bulk measurements and a neutron diffraction experiment with single crystals grown by hydrothermal synthesis. Magnetic phase transitions occur at $T = 14.0$ K and $T = 6.0$ K in $3R$-$AgFeO_2$ and $T = 17.0$ K and $T = 9.5$ K in $2H$-$AgFeO_2$ under zero magnetic field. Multistep metamagnetic phase transitions were observed in $3R$-$AgFeO_2$ in magnetization measurements up to 60 T, while a single phase transition occurs in $2H$-$AgFeO_2$. The ferroelectric polarization parallel and perpendicular to the triangular lattice plane appears below $T = 6.0$ K in $3R$-$AgFeO_2$, which is concomitant with the onset of the cycloid magnetic ordering with the propagation vector $\boldsymbol{k} = (-\frac{1}{2}, q, \frac{1}{2}; q \simeq 0.2)$ and the magnetic point group polar $m1'$. On the other hand, the ferroelectric polarization is absent even below the lower phase transition temperature in $2H$-$AgFeO_2$, which can be explained by the proper screw magnetic structure with $\boldsymbol{k} = (0, q, 0; q \simeq 0.4)$ and the nonpolar $2221'$ point group. Although the two-dimensional triangular lattice layers of Fe^{3+} are common in the two polytypes, the magnetic and ferroelectric properties are significantly different. The emergence of ferroelectric polarization which is not confined to be within the plane of the cycloid for $3R$-$AgFeO_2$ can be explained by the extended inverse Dzyaloshinskii-Moriya effect with two orthogonal components, $\boldsymbol{p}_1 \propto \boldsymbol{r}_{ij} \times [\boldsymbol{S}_i \times \boldsymbol{S}_j]$ and $\boldsymbol{p}_2 \propto \boldsymbol{S}_i \times \boldsymbol{S}_j$. Unlike other delafossite compounds, the $\boldsymbol{p}_2$ component is not allowed in the proper screw phase of $2H$-$AgFeO_2$ due to the symmetry restriction of the parent space group.

DOI: 10.1103/PhysRevB.99.064402

I. INTRODUCTION

Magnetoelectric multiferroic compounds, which possess ferroelectric and (anti)ferromagnetic orderings, have attracted much attention in last 15 years [1–3]. Delafossite family compounds ABO_2 (A = Cu, Ag, B = Cr, Fe) with the $R\bar{3}m$ space group have provided great opportunities to study the coupling mechanism between magnetic and ferroelectric orderings in multiferroics [4]. In the delafossites, there are various types of magnetic orderings including noncollinear structures coupled to ferroelectricity. The coupling mechanisms for noncollinear spin structures, which are called the inverse Dzyaloshinskii-Moriya (DM) effect [5,6] and the spin current mechanism [7], have been proposed by theoretical papers, showing that the electric dipole moments $\boldsymbol{p}$ generated by a pair of neighboring spins $\boldsymbol{S}_i$ and $\boldsymbol{S}_j$ are expressed as $\boldsymbol{p} \propto \boldsymbol{r}_{ij} \times [\boldsymbol{S}_i \times \boldsymbol{S}_j] (\equiv \boldsymbol{p}_1)$. In specific cases, such as the orthorhombic perovskite with the $Pbnm$ space group and a cycloid structure, $\boldsymbol{r}_{ij} \perp [\boldsymbol{S}_i \times \boldsymbol{S}_j]$, the theory can well explain the ferroelectric polarization [8,9].

In $CuFeO_2$ and $CuCrO_2$, however, the proper screw magnetic ordering also induces the ferroelectric polarization parallel to the vector product of neighboring spins, $\boldsymbol{p} || [\boldsymbol{S}_i \times \boldsymbol{S}_j]$, in spite of $\boldsymbol{p}_1 = 0$ due to $\boldsymbol{r}_{ij} || [\boldsymbol{S}_i \times \boldsymbol{S}_j]$ [10–18]. Kaplan and Mahanti have extended the inverse DM mechanism to general symmetry conditions [19], which can explain the polarization parallel to $\boldsymbol{S}_i \times \boldsymbol{S}_j$ in the proper screw ordering, which is orthogonal to the $\boldsymbol{p}_1$ components, $\boldsymbol{p} \propto \boldsymbol{S}_i \times \boldsymbol{S}_j (\equiv \boldsymbol{p}_2)$. In some other multiferroics with proper screw ordering, the ferroelectric polarization parallel to $\boldsymbol{S}_i \times \boldsymbol{S}_j$ has been reported [20–22]. The mechanism is applicable for the cycloid magnetic structure ($\boldsymbol{r}_{ij} \perp [\boldsymbol{S}_i \times \boldsymbol{S}_j]$) as well as the proper screw case. For example, the ferroelectric polarization parallel to $\boldsymbol{S}_i \times \boldsymbol{S}_j$ in addition to the dominant polarization along the trigonal axis has been reported in the cycloidal phase in $BiFeO_3$ [23].

The magnetic and dielectric properties of the silver delafossite ferrite $3R$-$AgFeO_2$ ($R\bar{3}m$) have been investigated in a previous work using a powder sample [24]. There are two magnetic phase transitions at $T = 15$ and 9 K in $3R$-$AgFeO_2$. A collinear spin-density-wave (SDW) ordering is stabilized for 9 K $\leqslant T \leqslant$ 15 K, while it turns into the cycloid ordering with spin components confined to the hexagonal [110]-[001] plane below $T = 9$ K. Although a ferroelectric polarization appears below the lower phase transition and the polarization direction was predicted to be the sum of the two orthogonal components, $\boldsymbol{p}_1$ and $\boldsymbol{p}_2$ [24], the direction of polarization was experimentally unclear due to only the $3R$-$AgFeO_2$ powder sample being available at that time.

*terada.noriki@nims.go.jp
†hirohiko@phys.chuo-u.ac.jp

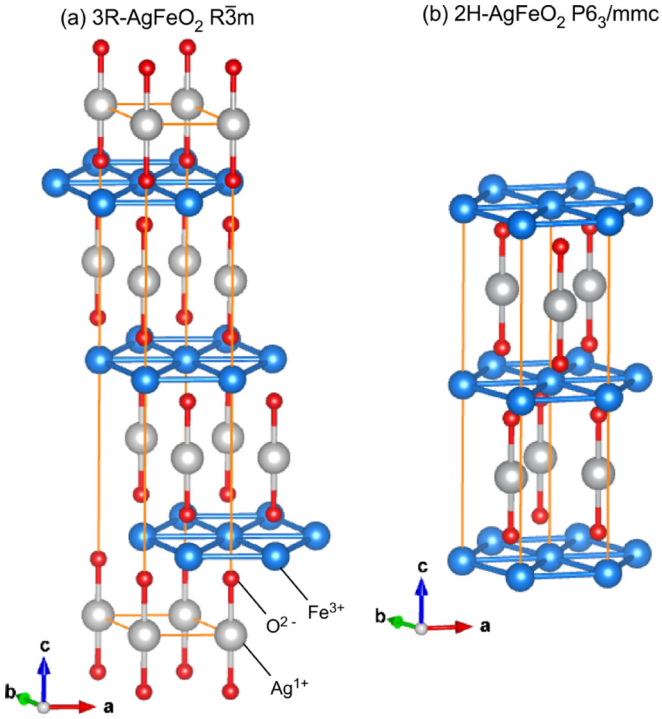

FIG. 1. Crystal structures of (a) $3R$-$AgFeO_2$ ($R\bar{3}m$) and (b) $2H$-$AgFeO_2$ ($P6_3/mmc$). The lattice parameters for $3R$-$AgFeO_2$ are $a = 3.0391$ Å, $c = 18.590$ Å, Ag(0,0,0), Fe(0,0,0.5), O(0,0,0.1112) [25], and those for $2H$-$AgFeO_2$ are $a = 3.039$ Å, $c = 12.395$ Å, Ag(1/3, 2/3, 0.25), Fe(0,0,0), O(1/3, 2/3, 0.0833) [26].

There is another polytype with the hexagonal space group $P6_3/mmc$, $2H$-$AgFeO_2$, with a crystal structure very similar to that of $3R$-$AgFeO_2$. As illustrated in Fig. 1, although the two-dimensional triangular lattice layers of Fe^{3+} are common in the two polytypes, the stacking sequences are different, ABCABC... in $3R$-$AgFeO_2$ and $AA'AA'$... in $2H$-$AgFeO_2$. The previous powder study of $2H$-$AgFeO_2$ argued that the difference in the parent space group, rhombohedral or hexagonal, affects the ferroelectric polarization at low temperature in $AgFeO_2$ significantly [27]. In $2H$-$AgFeO_2$, several magnetic phases exist, which are a SDW ($11\,K \leqslant T \leqslant 18\,K$), a proper screw ($T \leqslant 14\,K$), and a general spiral phase below $T = 5.5\,K$, which coexist with each other even at the lowest temperature. The emergence of ferroelectric polarization is concomitant with the onset of the general spiral order. The proper screw ordering does not generate the polarization in the hexagonal polytype $2H$-$AgFeO_2$, which is significantly different from the case in $3R$-CuBO_2 (B = Cr and Fe). However, the previous work could not determine the true ground state owing to the phase coexistence of the powder sample in $2H$-$AgFeO_2$ [27].

Recently, we succeeded in growing single crystals of both $3R$-$AgFeO_2$ and $2H$-$AgFeO_2$ by using the hydrothermal synthesis method. In the present study, we extend the powder studies [24,27] and clearly investigate the magnetic phase transitions and the difference in the ferroelectric polarization induced by the noncollinear orderings by using the single crystals of the two polytypes of $AgFeO_2$. We performed magnetization, dielectric permittivity, and pyroelectric current measurements and neutron diffraction experiments on single-crystal samples of $3R$-$AgFeO_2$ and $2H$-$AgFeO_2$.

II. EXPERIMENTAL DETAILS

Single crystals of $3R$-$AgFeO_2$ and $2H$-$AgFeO_2$ were grown using a hydrothermal method. In this process, the starting materials, Fe_2O_3 and Ag_2O, were sealed in a silver capsule with a small amount of RbOH. This mixture was kept at 650 °C and 150 MPa for 2 days. After the reaction, hexagonal plates of both $3R$-$AgFeO_2$ and $2H$-$AgFeO_2$ with a typical thickness of 0.5 mm, as shown in Figs. 2(a) and 2(b), were obtained. This result infers that these polytypes can be grown under very similar conditions. By single-crystal x-ray diffraction experiments, carried out at $T = 113$ K for $3R$-$AgFeO_2$ and $T = 293$ K for $2H$-$AgFeO_2$, we confirmed that these were single crystals [28]. The two polytypes can be distinguished by the difference in the diffraction patterns [29], for example, $L = 3n$ (n is an integer) in $3R$-$AgFeO_2$ and $L = 2n$ in $AgFeO_2$ along the c^* direction. X-ray Laue images are shown in Figs. 2(a) and 2(b). We confirmed that there is no ferromagnetic component caused by magnetic impurity, such as Fe_2O_3, by magnetization measurements on the single crystal.

Magnetization up to 6.0 T was measured using a magnetic property measurement system (Quantum Design, MPMS-XL). Magnetization at higher magnetic fields up to 60 T was measured using a pulsed magnet at the Institute for Solid State Physics (ISSP) at the University of Tokyo. Dielectric permittivity and pyroelectric current measurements were performed with a physical properties measurement system (Quantum Design, PPMS). The dielectric permittivity and pyroelectric current were determined using an *LCR* meter (Agilent, E4980A) and an electrometer (Keithley, 6517B), respectively. Frequencies of 100 kHz and 1 MHz were employed for the dielectric permittivity measurements. During pyroelectric current measurements, the sample was first cooled under a poling electric field up to ±800 kV/m, and subsequently, the pyroelectric current was recorded on warming in zero electric field. Integrating the current with respect to time gave the dielectric polarization. We confirmed that the sign of the dielectric polarization was reversed when reversing the poling electric field. For a pyroelectric current measurement under a pulsed magnetic field up to 40 T at ISSP, after cooling under poling electric field, we measured the current without electric field while sweeping a magnetic field. We applied magnetic fields along one of three equivalent [110] directions in the case of B_{ab} and along the hexagonal c axis in the case of B_c.

Single-crystal neutron diffraction measurements were carried out using the Wide angle In a Single Histogram (WISH) cold neutron time-of-flight diffractometer [30] at the ISIS facility of the Rutherford Appleton Laboratory (United Kingdom). The single crystal was mounted on a standard He cryostat with the hexagonal $[1\bar{1}0]$ axis vertical. Since the WISH diffractometer has a pair of wide coverage area detectors with ±15° in the vertical direction, we can provide access to the out of scattering plane of the hexagonal (H, H, L) [monoclinic $(2\bar{H}, K, H)$ in $3R$-$AgFeO_2$ and orthorhombic $(0, K, L)$ planes in $2H$-$AgFeO_2$]. We use monoclinic notation in $3R$-$AgFeO_2$ and orthorhombic

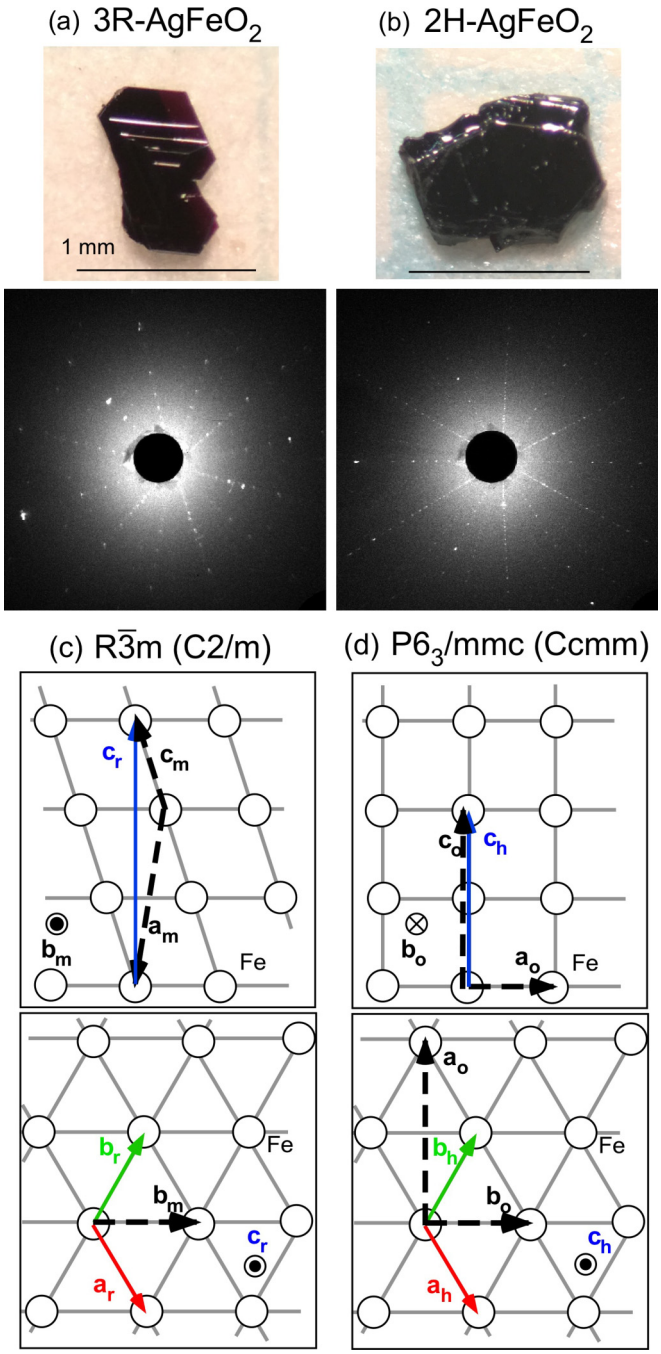

FIG. 2. Photographs and x-ray Laue images of the hexagonal c direction of the single crystals of (a) $3R$-$AgFeO_2$ and (b) $2H$-$AgFeO_2$. Relationship of the unit cell basis vectors above and below the magnetic phase transition temperatures: (c) $R\bar{3}m$ and $C2/m$ in $3R$-$AgFeO_2$ and (d) $P6_3/mmc$ and $Ccmm$ in $2H$-$AgFeO_2$ space groups. The subscripts r, m, h, and o denote unit vectors for $R\bar{3}m$ (hexagonal setting), $C2/m$, $P6_3/mmc$, and $Ccmm$, respectively.

notation in $2H$-$AgFeO_2$ unless otherwise specified. Because magnetic orderings lower the symmetries down to monoclinic in $3R$-$AgFeO_2$ and orthorhombic in $2H$-$AgFeO_2$ below magnetic phase transition temperatures, it is convenient to use these low-symmetry notations. Actually, in previous powder neutron diffraction experiments [24,27,31], nuclear peak splittings and broadenings indicated losing the threefold and sixfold rotational symmetry elements of $R\bar{3}m$ and $P6_3/mmc$ in $3R$-$AgFeO_2$ and $2H$-$AgFeO_2$, respectively. The results imply symmetry lowering down to at least the maximal nonisomorphic subgroup $C2/m$ in $3R$-$AgFeO_2$ and $Ccmm$ in $2H$-$AgFeO_2$, which takes into account only the coupling of the magnetic order parameter to the macroscopic strains. The relationships between the rhombohedral (hexagonal setting) and monoclinic bases and the hexagonal and orthorhombic bases are illustrated in Figs. 2(c) and 2(d). Crystal and magnetic structure refinements were performed using the FULLPROF program [32].

III. EXPERIMENTAL RESULTS

A. Magnetization

3R-AgFeO$_2$. Temperature dependences of magnetic susceptibility $\chi(T)$ under magnetic fields perpendicular to the hexagonal c axis (B_{ab}) and parallel to the c axis (B_c) up to 6 T for $3R$-$AgFeO_2$ are shown in Figs. 3(a) and 3(b). A small peak anomaly was observed at $T = 14$ K in both directions, while $\chi(T)$ exhibits a sharp drop at $T = 5.5$ K in $B_{ab} = 0.1$ T and $B_c = 0.1$ T. As reported in the previous powder study [24], these anomalies are expected to be the magnetic phase transitions from the paramagnetic phase to the incommensurate phase (ICM1) and from ICM1 to ICM2 phases. The phase transition temperatures, $T = 14$ and 5.5 K, of the single crystal are not perfectly consistent with those of the powder sample ($T = 15$ and 9 K) [24]. Although the inconsistency between powder and single-crystal samples is not fully understood, the difference in the sample quality might affect the stability of magnetic ordering in $3R$-$AgFeO_2$, similar to what is seen in other frustrated systems [33–35]. The higher transition temperature is independent of the magnetic fields. While the lower transition temperature is not affected by B_{ab}, it gradually decreases with increasing B_c, as illustrated by the dotted lines in Figs. 3(a) and 3(b).

We measured the magnetization processes at $T = 1.3$ K in B_{ab} and B_c in $3R$-$AgFeO_2$, which are shown in Figs. 4(a) and 4(b). The magnetization exhibits no clear anomaly in B_{ab} up to 60 T apart from a slight change in the slope around 40 T shown in Fig. 4(a). On the other hand, the multistep metamagnetic behavior was observed in B_c. The critical fields are $B_c = 12.5$ T ($\equiv B_{c1}$), 27.0 T ($\equiv B_{c2}$), 38.0 T ($\equiv B_{c3}$), and 49.5 T ($\equiv B_{c4}$), The first, second, and fourth field-induced phase transitions show hysteresis, indicating first-order phase transitions, while the third one has no hysteresis, suggesting a second-order transition. The magnetization values are $\sim 1\mu_B$ (1/5 of $5\mu_B$ of Fe^{3+}) for $B_{c1} \leqslant B_c \leqslant B_{c2}$ and $\sim 1.67\mu_B$ (1/3 of $5\mu_B$) for $B_{c2} \leqslant B_c \leqslant B_{c3}$. Making a comparison with the similar magnetization process of the well-studied $3R$-$CuFeO_2$ case, we can expect the collinear five sublattice (5SL) $\uparrow\uparrow\uparrow\downarrow\downarrow$ and the three sublattice (3SL) $\uparrow\uparrow\downarrow$ for $B_{c1} \leqslant B_c \leqslant B_{c2}$ and $B_{c2} \leqslant B_c \leqslant B_{c3}$, respectively. The details of the 5SL and 3SL structures are described in previous papers [36,37]. For $B_{c3} \leqslant B_c \leqslant B_{c4}$, we can expect a noncollinear canted 3SL from the linearly increasing magnetization, while the conical structure was predicted for $B_c \geqslant B_{c4}$ [38]. The magnetization

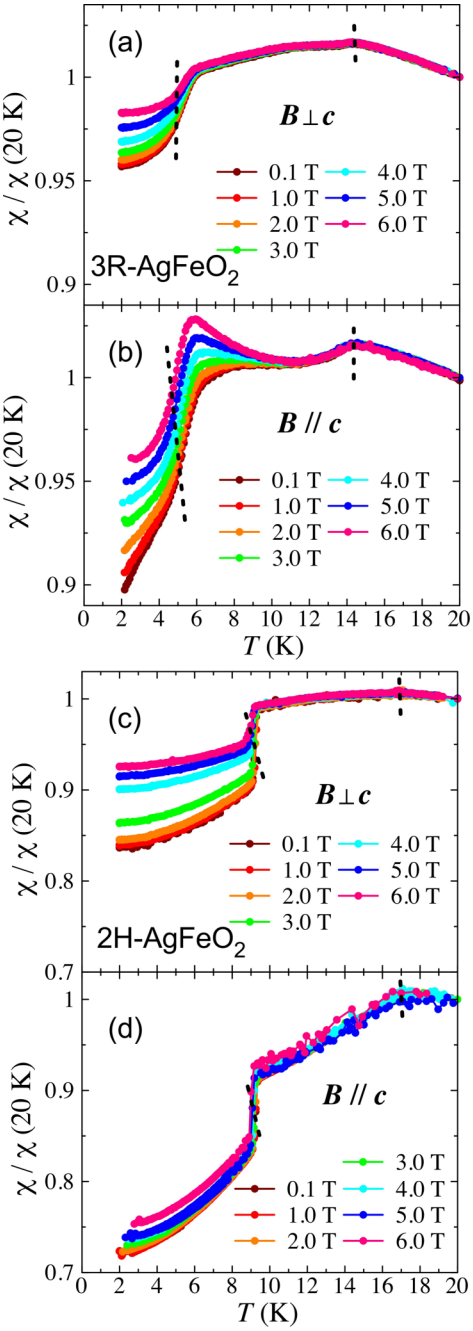

FIG. 3. Temperature dependence of magnetic susceptibility under magnetic fields (a) perpendicular to the hexagonal c axis and (b) parallel to the c axis in $3R$-$AgFeO_2$. (c) and (d) The data for $2H$-$AgFeO_2$. These data were normalized to the value at $T = 20$ K. The dotted lines show the magnetic phase transition temperatures.

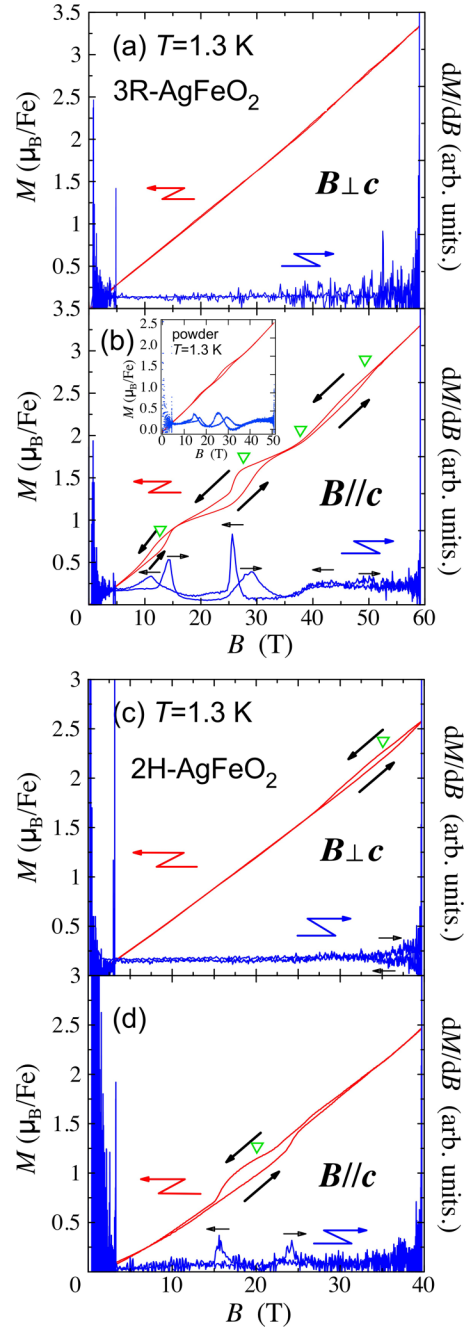

FIG. 4. Magnetization processes and the derivative of magnetization with respect to the magnetic field (dM/dB) under pulsed magnetic field (a) perpendicular to the hexagonal c axis and (b) parallel to the c axis at $T = 1.3$ K in $3R$-$AgFeO_2$. (c) and (d) The data for $2H$-$AgFeO_2$. The inset in (b) shows the data measured with a powder sample of $3R$-$AgFeO_2$. Triangles show the phase transition fields.

process for the powder sample also exhibits these anomalies with broader peak shapes in dM/dB, as shown in the inset of Fig. 4(b). A detailed comparison of the magnetization process of $3R$-$AgFeO_2$ with $3R$-$CuFeO_2$ is discussed in Sec. IV.

2H-AgFeO$_2$. Figures 3(c) and 3(d) show the temperature dependences of magnetization in B_{ab} and B_c up to 6 T in $2H$-$AgFeO_2$. A small peak and a steep drop in anomalies were found at $T = 17$ K and $T = 9.4$ K at $B_{ab} = B_c = 0.1$ T, respectively. As also seen in the case of $3R$-$AgFeO_2$, the phase transition temperatures of the single-crystal sample are slightly lower than those of the powder sample reported in a previous paper (18 and 11 K) in $2H$-$AgFeO_2$ [27]. It should be noted that the phase transitions observed in the magnetization data of the single crystal are much clearer than those of the previous powder data with the phase coexistence. The

magnetic fields B_{ab} and B_c up to 6 T do not affect the phase transition temperatures significantly.

The magnetization processes of $2H$-$AgFeO_2$ are completely different from those of $3R$-$AgFeO_2$, which are shown in Figs. 4(c) and 4(d). This difference infers that exchange parameters are significantly different from those of $3R$-$AgFeO_2$. In B_{ab}, the metamagnetic phase transition was observed around $B_{ab} = 35$ T, which has a large hysteresis. The data for B_c also exhibit a single phase transition with large hysteresis around $B_c = 20$ T. Unlike $3R$-$AgFeO_2$, magnetization plateaus are not seen in $2H$-$AgFeO_2$, which suggests that noncollinear magnetic orderings are realized in the high-magnetic-field phases $B_{ab} \geqslant 35$ T and $B_c \geqslant 20$ T as well as in the lower field phase.

B. Dielectric properties

3R-AgFeO$_2$. We measured the dielectric permittivity and the pyroelectric current associated with the magnetic phase transitions. In $3R$-$AgFeO_2$, we observed step anomalies at $T = 14$ K and $T = 5.5$ K in the dielectric permittivity along directions both parallel and perpendicular to the *ab* plane, as shown in Figs. 5(a) and 5(b). We observed the ferroelectric polarizations below $T = 5.5$ K for both directions, as shown in Fig. 5(c). Although the direction of polarization was unknown in the previous powder work [24], we found that the polarization contains the two components P_{ab} and P_c in the present single-crystal study. The polarization values are $P_{ab} \sim 300\ \mu C/m^2$ and $P_c \sim 100\ \mu C/m^2$, which do not reach the maximum values with the poling electric field up to 267 and 800 kV/m, respectively, as shown in the inset of Fig. 5(c). By application of magnetic field at 4.2 K, the ferroelectric polarization disappears at $B_c \simeq 13$ T [Fig. 5(d)], which is associated with the phase transition from the ICM2 phase to the collinear 5SL ↑↑↑↓↓ phase with the nonpolar point group.

2H-AgFeO$_2$. In contrast, we did not observe any anomalies around the phase transition temperature in the dielectric permittivity, suggesting that spin-lattice coupling is weak in $2H$-$AgFeO_2$ compared with that in $3R$-$AgFeO_2$. In the pyroelectric current measurements, we did not find any peak anomaly around the magnetic phase transition temperatures for $2H$-$AgFeO_2$ within the experimental accuracy.

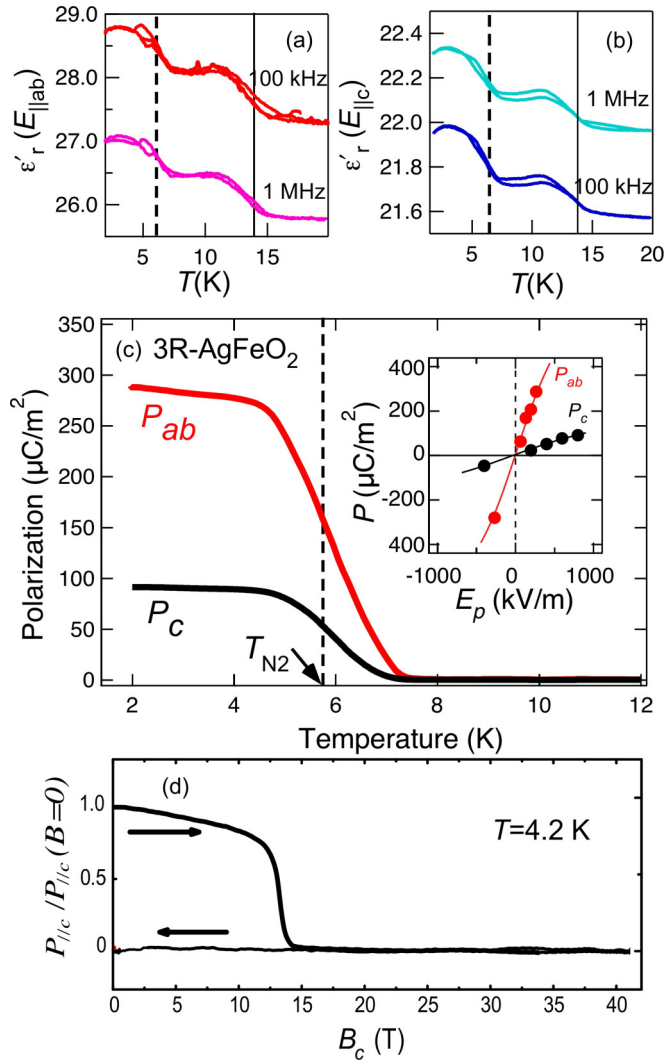

FIG. 5. Temperature dependence of dielectric permittivity (a) perpendicular to the hexagonal c axis and (b) parallel to the c axis in $3R$-$AgFeO_2$. (c) Temperature dependence of electric polarization perpendicular to the hexagonal c axis and parallel to the c axis, which was measured after poling in electric field, 267 and 800 kV/m, respectively. The inset in (c) is the poling electric field dependence of electric polarization along both directions. (d) Magnetic field dependence of the electric polarization along the c axis at $T = 4.2$ K.

C. Neutron diffraction

3R-AgFeO$_2$. The temperature dependence of magnetic neutron diffraction profiles along the reciprocal lattice $[\bar{1}, K, \frac{1}{2}]$ line is shown in Fig. 6(a). The diffraction peak assigned as the incommensurate $(\bar{1}, q, \frac{1}{2})$ with $q \simeq 0.4$ appears below $T = 14$ K, which corresponds to the higher phase transition from the paramagnetic phase to the ICM1 phase. The wave number q significantly depends on temperature from $q = 0.39$ at $T = 14$ K and remains at $q = 0.41$ below $T \sim 7$ K, as clearly seen in Fig. 7(b). The temperature-dependent propagation vector in the ICM1 phase, $\boldsymbol{k} = (\bar{1}, q, \frac{1}{2})$, is consistent with that observed for the powder sample [24], suggesting that the collinear SDW structure is realized in the single-crystal sample. An additional reflection with q very close to $q \simeq 0.39$ appears below 10 K in the ICM1 phase, indicating that a magnetic ordering with a slightly different $\boldsymbol{k}$ vector appears. This is similarly seen as the peak broadening observed in the powder sample [24]. The coexistence behavior has also been found near the first-order phase transition for another frustrated system, which can be explained by the strong competition between frustrated exchange interaction and thermal fluctuations [39].

With further decreasing temperature, the intensity of reflections for the ICM1 phase significantly decreases below $T = 6.0$ K, and the reflection persists at the lowest temperature, $T = 1.5$ K. At the same time, the diffraction peak at $(\frac{1}{2}, 0.205, -\frac{1}{2})$ is observed [Figs. 6(b) and 7(a)] below $T = 6.0$ K, which corresponds to the phase transition from the ICM1 to ICM2 phase. Here $\boldsymbol{k} = (-\frac{1}{2}, q, \frac{1}{2})$ is consistent with that in the ICM2 phase observed in the powder sample

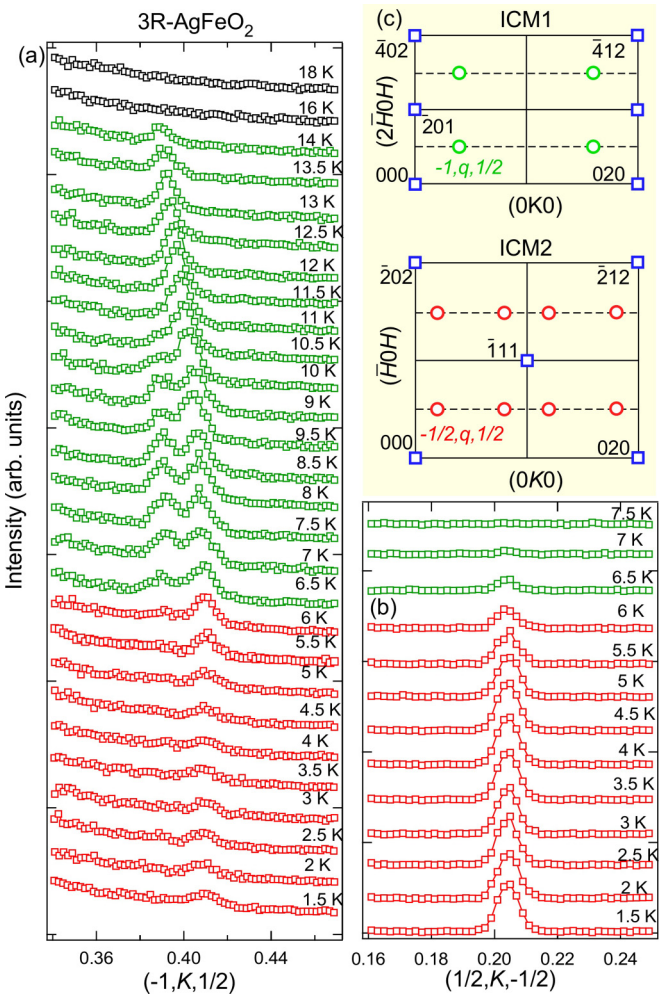

FIG. 6. Temperature dependence of the neutron diffraction profile along the reciprocal lattice lines (a) $[\bar{1}, K, \frac{1}{2}]$ and (b) $[\frac{1}{2}, q, \frac{\bar{1}}{2}]$ in $3R$-$AgFeO_2$. (c) Schematic illustrations of the reciprocal lattice planes, $(2\bar{H}, K, H)$ for the ICM1 phase and $(\bar{H}, K, H)$ for the ICM2 phase. Squares and circles denote nuclear and magnetic reflections points.

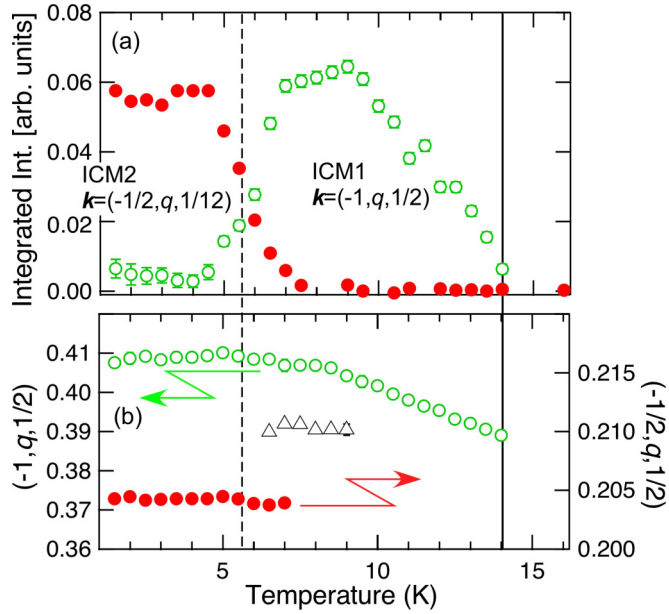

FIG. 7. (a) Temperature dependence of the integrated intensity of magnetic reflections indexed by $\boldsymbol{k} = (\bar{1}, q, \frac{1}{2})$ and $\boldsymbol{k} = (\frac{\bar{1}}{2}, q, \frac{1}{2})$ in $3R$-$AgFeO_2$. (b) Temperature dependence of the incommensurate wave number (b component) in the $\boldsymbol{k}$ vector.

[24]. The magnetic Bragg peak positions are drawn on the reciprocal lattice planes shown in Fig. 6(c). The wave number q in the ICM2 phase is independent of temperature, as shown in Fig. 7(b). From the consistency in the $\boldsymbol{k}$ vector in the ICM2 phase between single-crystal and powder samples, it can naturally be thought that the cycloid magnetic ordering is realized in the ICM2 phase in the single-crystal sample. Magnetic structure analysis in $3R$-$AgFeO_2$ could not be performed due to the lack of a sufficient number of observable magnetic reflections in the present experiment.

2H-AgFeO$_2$. The temperature dependence of the neutron diffraction profile for $2H$-$AgFeO_2$ is shown in Figs. 8(a) and 8(b). Below $T = 17$ K, a magnetic reflection starts to appear at $(0, 0.4, -1)$, corresponding to the magnetic phase transition from the paramagnetic phase to the ICM1 phase in $2H$-$AgFeO_2$. The $\boldsymbol{k}$ vector can be determined to $\boldsymbol{k} = (0, q, 0)$ in the ICM1 phase, which is consistent with the SDW ordering of the powder sample [27]. We observe the strong temperature dependence in q in the ICM1 phase, as shown in Figs. 8(a) and 9(b).

Below $T = 9.5$ K, a set of magnetic reflections is clearly found at $(0, 0.4, -1)$ and $(0, 0.6, -1)$. Instead of this, the reflections of the ICM1 phase varnishes, corresponding to the phase transition from the ICM1 to ICM2 phase [Figs. 7(b) and 8(b)]. We can define the $\boldsymbol{k}$ vector as $\boldsymbol{k} = (0, q, 0)$ with temperature-independent $q = 0.4$ [Fig. 7(b)]. In the previous powder experiment, two magnetic phases coexisted at low temperature, which included the proper screw phase (ICM2) with $\boldsymbol{k} = (0, q, 0)$, with $q = 0.4$, and the general spiral phase (ICM3) with $\boldsymbol{k} = (q_a, q_b, q_c)$ [27]. The $\boldsymbol{k}$ vector observed in the present study is in agreement with the proper screw phase in the powder study. The ICM3 phase seen in the powder sample was not observed in the present single-crystal experiment, meaning that the single magnetic ground state of the ICM2 phase is realized in the single crystal of $2H$-$AgFeO_2$. The ICM3 phase might be induced by a small amount of impurity in the powder sample [27].

In order to determine the magnetic structure in the ICM2 phase of $2H$-$AgFeO_2$, we performed the magnetic structure analysis using observed magnetic and nuclear reflections at $T = 1.5$ K. We compared the experimental data, corrected by the Lorentz factor, with magnetic structure factors calculated from noncollinear spin models. It should be noted that the reciprocal lattice points where the observed satellite reflections start are at not only the symmetry-allowed $H + K = 2n$ (n is an integer) but also the forbidden $H + K = 2n + 1$ in the $Ccmm$ space group for the ICM2 phase. This observation implies the presence of structure distortion violating the C-centering condition and indicates a further symmetry reduction at least down to $Pmma$. The distortion can be expressed by the $Y1+$ irreducible representation (IR; in the ISODISTORT notations [40,41]). The symmetry lowering

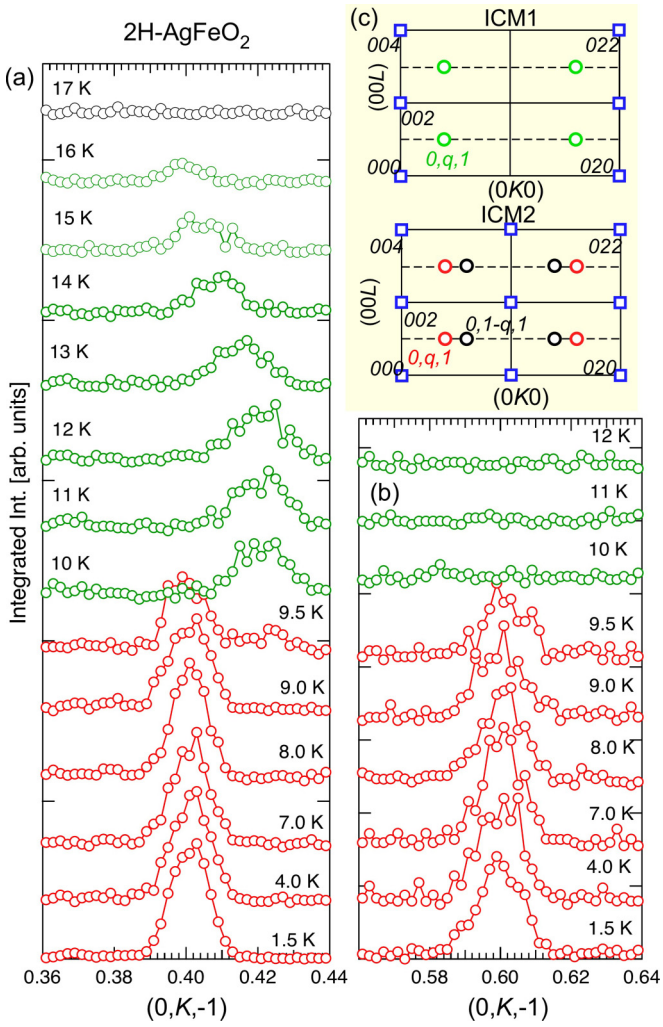

FIG. 8. Temperature dependence of the neutron diffraction profile along the reciprocal lattice lines (a) $[0, K, \bar{1}]$ and (b) $[0, q, \bar{1}]$ in $2H$-$AgFeO_2$. (c) Schematic illustrations of the reciprocal lattice planes, $(0, K, L)$ for the ICM1 and ICM2 phases. Squares and circles denote nuclear and magnetic reflections points.

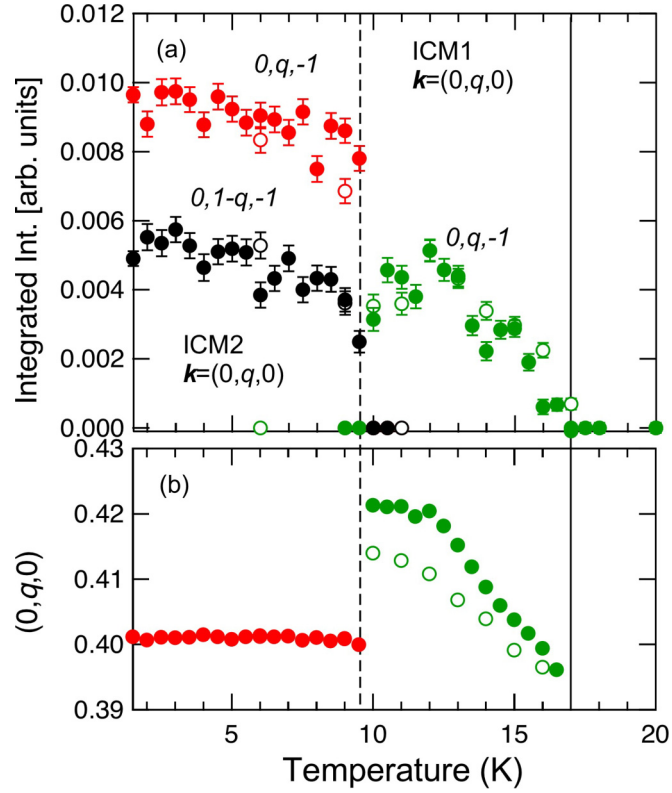

FIG. 9. (a) Temperature dependence of the integrated intensity of magnetic reflections indexed by $\boldsymbol{k} = (0, q, 0)$ in $2H$-$AgFeO_2$. (b) Temperature dependence of the incommensurate wave number (b component) in the $\boldsymbol{k}$ vector. Solid and open symbols denote the data measured with warming and cooling processes, respectively.

should make two Fe^{3+} sites, (0,0,0) and $(\frac{1}{2}, \frac{1}{2}, 0)$ [or (0,0,1) and $(\frac{1}{2}, \frac{1}{2}, \frac{1}{2})$] in the orthorhombic unit cell, inequivalent, leading to the independent initial phase in the incommensurate modulation at the two sites. The phase difference between them is defined to be δ. As shown in Figs. 10(a) and 10(b), the magnetic structure in the ICM2 phase of $2H$-$AgFeO_2$ has been determined to the proper screw structure with ellipsoidal distortion with the reliability factor $R_F = 7.8\%$. The order parameter of the proper screw structure can be expressed by a combination of time-odd IRs of the $Pmma$ space group, $mDT_3 \oplus mDT_4$ (in the ISODISTORT notations [40,41]). The refined parameters are the amplitudes of magnetic moments along the a axis and c axis, $M_a = 1.9\mu_B$ and $M_c = 3.2\mu_B$, and the initial phase shift $\delta = 0.39\pi$. The refined δ value corresponds to the ferromagnetic arrangement between (0,0,0) and $(\frac{1}{2}, \frac{1}{2}, 0)$ and $(0, 0, \frac{1}{2})$ and $(\frac{1}{2}, \frac{1}{2}, \frac{1}{2})$ [Fig. 10(b)]. The determined magnetic structure is consistent with the result obtained in the powder study [27]. The symmetry of the ICM2 phase is also described by the $P2_1221'(0, 0, \gamma)00ss$, $\gamma = q$ magnetic superspace group [40,41], indicating that the magnetic order parameter breaks all the mirror plane symmetries but keeps the twofold rotational symmetries along the three orthogonal directions, resulting in the nonpolar magnetic point group $2221'$. This is consistent with the absence of the electric polarization below $T = 9.5$ K. The magnetic structure of the ICM2 phase determined in the present work for the $2H$-$AgFeO_2$ polytype is similar to the magnetic polar phase found in $3R$-$CuFe_{1-x}Ga_xO_2$ [4,13,15]. However, the magnetic point groups are different from each other, nonpolar $2221'$ in $2H$-$AgFeO_2$ and polar $21'$ in $3R$-$CuFe_{1-x}Ga_xO_2$. The difference relates to the hexagonal and rhombohedral parent symmetries, resulting in the absence and emergence of the ferroelectricity, respectively.

IV. DISCUSSION

A. Exchange interactions and anisotropy

$3R$-$AgFeO_2$ exhibits multistep magnetization changes through the application of magnetic field along the hexagonal c axis, which is very similar to that of the other delafossite ferrite $3R$-$CuFeO_2$ apart from a quantitative difference in critical fields [37,38,42,43]. Therefore, we can thus infer that $3R$-$AgFeO_2$ is considered to be a triangular lattice antiferromagnet with exchange interactions up to third-nearest neighbors [44] with exchange and anisotropic parameters slightly modified from those in $3R$-$CuFeO_2$. The critical

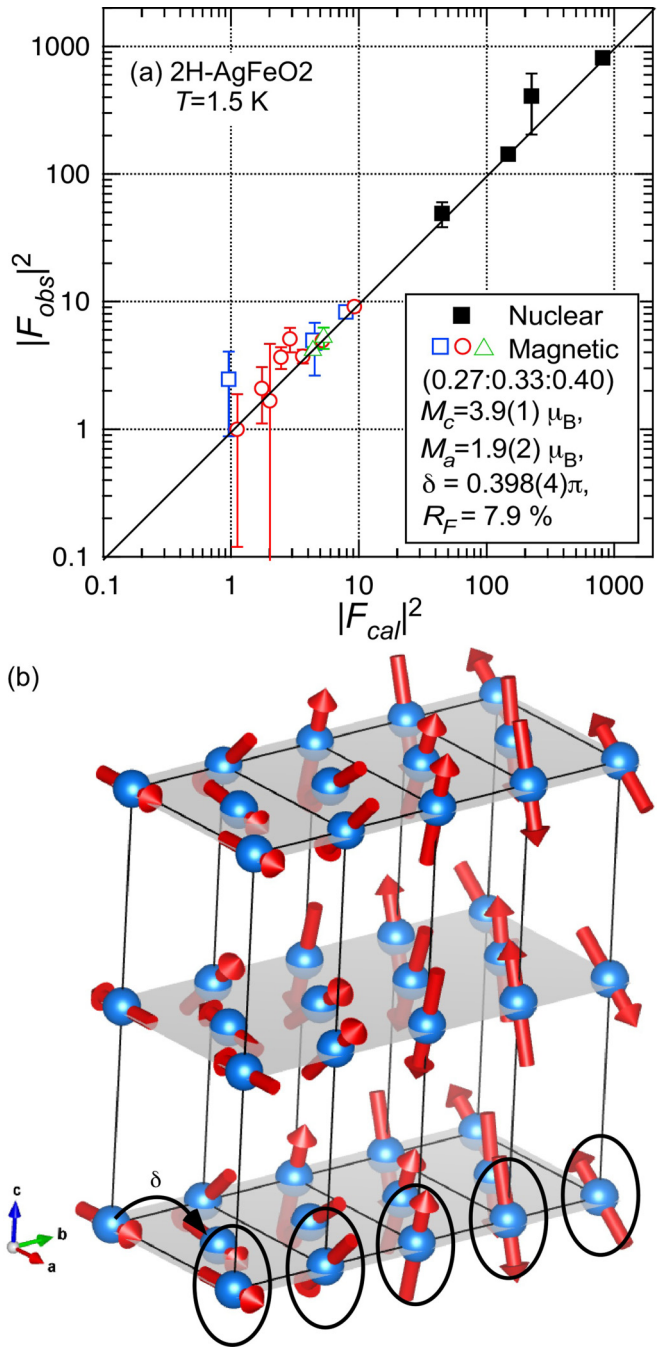

FIG. 10. (a) Result of the refinement for the data acquired at $T = 1.5$ K in $2H$-$AgFeO_2$. The open and solid symbols denote magnetic and nuclear reflections, and the difference in the symbols for magnetic data corresponds to different domains. The refined magnetic structure parameters, magnetic domain population, magnetic moments M_c and M_a, initial phase shift δ, and reliability factor R_F, are listed in the inset. (b) Illustrations of the determined magnetic structure, proper screw structure with ellipsoidal distortion for the ICM2 phase in $2H$-$AgFeO_2$.

magnetic fields for $3R$-$AgFeO_2$ and $3R$-$CuFeO_2$ are summarized in Table I. From the magnetization process in $3R$-$AgFeO_2$, we can expect the critical magnetic field where the magnetization reaches $5\mu_B$ of Fe^{3+} to be ∼85 T (defined as B_{c5}) by extrapolating the magnetization slope above $B_c =$ 50 T. Therefore, the total antiferromagnetic exchange interaction in $3R$-$AgFeO_2$ is larger than $3R$-$CuFeO_2$ with $B_{c5} = 75$ T, which is consistent with the larger Weiss temperature value of $\Theta = -140$ K in $3R$-$AgFeO_2$ compared with -90 K in $3R$-$CuFeO_2$. This tendency is also seen in the critical fields, B_{c2} and B_{c3}, as shown in Table I.

In contrast, we found some differences in the critical fields for B_{c0}, B_{c1}, and B_{c4}, which cannot be explained by the overall shift in exchange energy between the two compounds. Firstly, a spin-flop phase transition seen at $B_{c0} = 7$ T in $3R$-$CuFeO_2$ was not observed in $3R$-$AgFeO_2$. Reflecting the collinear, ↑↑↓↓, magnetic ground state in zero field, $3R$-$CuFeO_2$ shows a zero-magnetization plateau up to $B_c = 7$ T, followed by a spin-flop phase transition to the noncollinear proper screw phase with a finite gradient of magnetization. For $3R$-$AgFeO_2$, the noncollinear cycloid ordering in zero field gives a linear increasing of magnetization. The spin-flop transition is caused by competition between the easy-axis anisotropy and Zeeman energy, suggesting the anisotropy in $3R$-$AgFeO_2$ is smaller than that in $3R$-$CuFeO_2$, leading to the disappearance of the collinear ground state in zero field and spin-flop transition in $3R$-$AgFeO_2$.

Second, B_{c1} and B_{c4} in $3R$-$AgFeO_2$ are smaller than those of $3R$-$CuFeO_2$ in spite of the larger overall antiferromagnetic exchange interaction in $3R$-$AgFeO_2$. At B_{c1}, a magnetic phase transition occurs from the noncollinear cycloid in $3R$-$AgFeO_2$ and proper screw in $3R$-$CuFeO_2$ to the collinear 5SL (↑↑↑↓↓) phase. At B_{c4}, a phase transition occurs from the noncollinear canted 3SL to the conical spin state, as shown in Ref. [38]. Since phase transitions at both B_{c1} and B_{c4} are associated with either a noncollinear to collinear or one noncollinear to another noncollinear spin state, we can infer that the anisotropy energy is also an important factor for the critical field values. In $3R$-$CuFe_{1-x}X_xO_2$ (X = Al or Ga) with chemical doping, similar behaviors are seen, like the disappearance of the spin-flop phase transition at B_0 and the critical field reduction for B_{c1} and B_{c4}. In $3R$-$CuFe_{0.085}Al_{0.015}O_2$, the critical fields are the smaller values, $B_{c1} = 11.5$ T and $B_{c4} =$ 48 T [47]. Actually, in inelastic neutron scattering studies, the single-ion anisotropy constant D is reduced from 0.064 meV in $3R$-$CuFeO_2$ to 0.007 meV in $3R$-$CuFe_{0.985}Ga_{0.035}O_2$ [48,49]. Therefore, we can expect that the anisotropy energy in $3R$-$AgFeO_2$ is also weaker than that in $3R$-$CuFeO_2$. To further understand the exchange interactions and anisotropy, inelastic neutron scattering and electron spin resonance studies for $3R$-$AgFeO_2$ are needed.

For $2H$-$AgFeO_2$, in spite of almost the same exchange networks in the triangular lattice plane as in $3R$-$AgFeO_2$, the magnetization processes are completely different from each other. The nearest-neighbor exchange interaction $J1$ is known as the sum of Fe-O-Fe ∼90° antiferromagnetic superexchange and Fe-Fe direct ferromagnetic exchange interactions in the delafossite system [33]. Considering the Fe-O-Fe bond angle and Fe-Fe distance have nearly the same values, 96.54° and 3.039 Å in $2H$-$AgFeO_2$ [27] and 96.5° and 3.033 Å in $3R$-$AgFeO_2$ [24,31], we can expect almost the same $J1$ value. However, for the next-nearest neighbor $J2$, the third-nearest-neighbor interactions $J3$ in the triangular lattice plane, and the interlayer exchange interactions, these exchange paths are unknown and are expected to be much

TABLE I. List of critical magnetic fields and Weiss temperature for $3R$-$CuFeO_2$ and $3R$-$AgFeO_2$.

	B_{c0}(T)	B_{c1}(T)	B_{c2}(T)	B_{c3}(T)	B_{c4}(T)	B_{c5}(T)	Θ(K)	References
$3R$-$CuFeO_2$	7	13	20	34	54	75	−90 [45]	[37,38,42,43]
$3R$-$AgFeO_2$		12.5	27	38	49.5	85[a]	−140 [46]	This work

[a]The critical field B_{c5} was predicted by extrapolating the experimental data above $B_c = 50$ T in $3R$-$AgFeO_2$.

more complex than in the case of $J1$. Therefore, the difference in the stacking sequence of the triangular lattice layers along the hexagonal c axis between $2H$-$AgFeO_2$ and $3R$-$AgFeO_2$ is considered to significantly affect those exchange interactions, leading to the completely different magnetization process in $2H$-$AgFeO_2$.

B. Ferroelectric polarization

Let us discuss the direction of ferroelectric polarization in $3R$-$AgFeO_2$ and the absence of polarization in $2H$-$AgFeO_2$. In the present experiments, ferroelectric polarization with two components, P_{ab} and P_c, was observed in the ICM2 phase of $3R$-$AgFeO_2$, which is concomitant with the onset of the cycloid magnetic ordering with spins in the bc_h plane (c_h is the hexagonal c axis) and $m1'$ magnet point group. In contrast, the electric polarization was not observed in the proper screw phase (ICM2), with spins in the ac plane and $2221'$, in $2H$-$AgFeO_2$. As mentioned in the Introduction, in the well-known spin current [7] and inverse DM [5,6] theories, the polarization is expressed by $\boldsymbol{p}_1 \propto \boldsymbol{r}_{ij} \times (\boldsymbol{S}_i \times \boldsymbol{S}_j)$ and is expected to be perpendicular to both $\boldsymbol{r}_{ij}$ and $\boldsymbol{S}_i \times \boldsymbol{S}_j$. When a crystal has neither a mirror plane containing $\boldsymbol{r}_{ij}$ nor an n-fold rotation axis perpendicular to $\boldsymbol{r}_{ij}$, the electric polarization can be expected to be parallel to the cross product, $\boldsymbol{p} \propto \boldsymbol{S}_i \times \boldsymbol{S}_j (\equiv \boldsymbol{p}_2)$, via the inverse DM effect, as proposed by Kaplan and Mahanti [19]. This symmetry condition can also be explained by the fact that a crystal belongs to a ferroaxial point group [22]. In the case of $3R$-$AgFeO_2$ with $R\bar{3}m$, the magnetic propagation vector, such as $(q, q, 0)$ in the hexagonal basis, breaks the threefold rotational symmetry and lowers the symmetry to the monoclinic $C2/m$. It is convenient to use the extended $\boldsymbol{k}$-vector group to discuss the symmetry-allowed components of the spin-induced polarization [4,24]. The $C2/m$ space group with the ferroaxial point group, $2/m$, does not possess a mirror plane containing $\boldsymbol{r}_{ij}$ and an n-fold rotation axis perpendicular to $\boldsymbol{r}_{ij}$, leading to making the $\boldsymbol{p}_2$ component allowed. Actually, the observations of P_c and P_{ab} in the ICM2 phase of $3R$-$AgFeO_2$ are in agreement with the $\boldsymbol{p}_1$ and $\boldsymbol{p}_2$ components, respectively, as illustrated in Fig. 11(a). In contrast, in $2H$-$AgFeO_2$, the parent space group is $P6_3/mmc$, and the extended wave vector group of $(q, q, 0)$ is orthorhombic, $Ccmm$ (nonferroaxial), which has mirror planes containing $\boldsymbol{r}_{ij}$ and twofold rotation axes perpendicular to $\boldsymbol{r}_{ij}$. In this case, the second term, $\boldsymbol{p}_2$, is not allowed. Taking into account that the proper screw ordering has $\boldsymbol{S}_i \times \boldsymbol{S}_j$ parallel to $\boldsymbol{r}_{ij}$ and the $\boldsymbol{p}_1$ term is also zero, we can expect the absence of ferroelectricity in the ICM2 phase of $2H$-$AgFeO_2$, as the polarization was not observed in the present experiment [Fig. 11(b)].

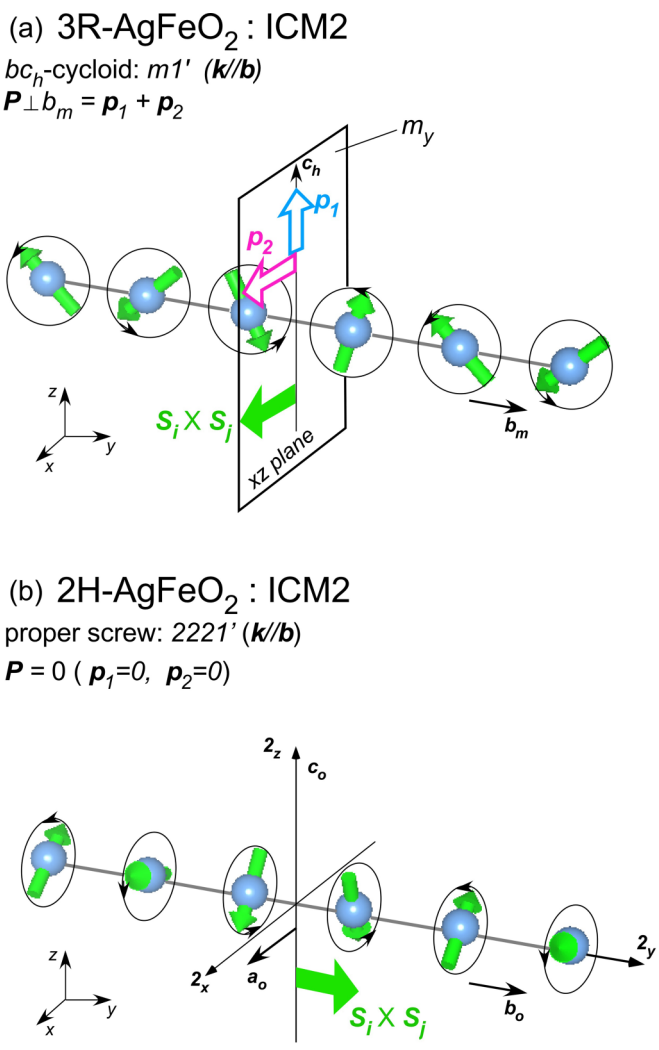

FIG. 11. Schematic illustrations representing the relationships between noncollinear spin modulation along the b axis and the electric polarization directions determined by the extended inverse DM mechanism [19], $\boldsymbol{p}_1 \propto \boldsymbol{r}_{ij} \times [\boldsymbol{S}_i \times \boldsymbol{S}_j]$ and $\boldsymbol{p}_2 \propto \boldsymbol{S}_i \times \boldsymbol{S}_j$, for (a) the cycloid phase in $3R$-$AgFeO_2$ and (b) the proper screw phase in $2H$-$AgFeO_2$.

V. CONCLUSION

In conclusion, we have investigated magnetic and dielectric properties of rhombohedral $3R$-$AgFeO_2$ and hexagonal $2H$-$AgFeO_2$ by using magnetic and dielectric bulk measurements and neutron diffraction experiments with single crystals grown by hydrothermal synthesis. Although the two-dimensional triangular lattice layers of Fe^{3+} are common in the two polytypes, the magnetic and ferroelectric properties are significantly different. The magnetization process in $3R$-$AgFeO_2$ exhibits 1/5 and 1/3 magnetization plateaus similar to those of $3R$-$CuFeO_2$, while that of $2H$-$AgFeO_2$ is completely different. Therefore, $3R$-$AgFeO_2$ is considered to be a triangular lattice antiferromagnet with exchange interactions up to third-nearest neighbors with exchange and anisotropic

parameters slightly modified from those in $3R$-$CuFeO_2$. On the other hand, in $2H$-$AgFeO_2$, the exchange interactions are significantly modified by the difference in the stacking sequence of the triangular lattice plane. Moreover, the ferroelectric polarization components, parallel and perpendicular to the hexagonal c axis, were observed in the cycloid phase in $3R$-$AgFeO_2$, as predicted in the generalized inverse DM mechanism including $\boldsymbol{p}_1 \propto \boldsymbol{r}_{ij} \times (\boldsymbol{S}_i \times \boldsymbol{S}_j)$ and $\boldsymbol{p}_2 \propto \boldsymbol{S}_i \times \boldsymbol{S}_j$. Unlike $3R$-$CuFeO_2$, the ferroelectric polarization is absent in the proper screw phase in $2H$-$AgFeO_2$ since the $\boldsymbol{p}_2$ term is not allowed in the case of the hexagonal parent space group.

ACKNOWLEDGMENTS

The images shown in Figs. 1, 10, and 11 were depicted using the VESTA [50] software program developed by K. Momma. This work was supported by JSPS KAKENHI Grants (No. 15H05433, 16K05413 and 17KK0099), JST-Mirai Program Grant Number JPMJMI18A3, Japan, and the TUMOCS project, which has received funding from the European Union Horizon 2020 Research and Innovation Program under the Marie Sklodowska-Curie grant agreement (Grant No. 645660).

[1] T. Kimura, T. Goto, H. Shintani, K. Ishizaka, T. Arima, and Y. Tokura, Nature (London) **426**, 55 (2003).
[2] S.-W. Cheong and M. Mostovoy, Nat. Mater. **6**, 13 (2007).
[3] Y. Tokura and S. Seki, Adv. Mater. **22**, 1554 (2010).
[4] N. Terada, J. Phys.: Condens. Matter **26**, 453202 (2014).
[5] M. Mostovoy, Phys. Rev. Lett. **96**, 067601 (2006).
[6] I. A. Sergienko and E. Dagotto, Phys. Rev. B **73**, 094434 (2006).
[7] H. Katsura, N. Nagaosa, and A. V. Balatsky, Phys. Rev. Lett. **95**, 057205 (2005).
[8] M. Kenzelmann, A. B. Harris, S. Jonas, C. Broholm, J. Schefer, S. B. Kim, C. L. Zhang, S.-W. Cheong, O. P. Vajk, and J. W. Lynn, Phys. Rev. Lett. **95**, 087206 (2005).
[9] T. Arima, A. Tokunaga, T. Goto, H. Kimura, Y. Noda, and Y. Tokura, Phys. Rev. Lett. **96**, 097202 (2006).
[10] T. Kimura, J. C. Lashley, and A. P. Ramirez, Phys. Rev. B **73**, 220401(R) (2006).
[11] S. Kanetsuki, S. Mitsuda, T. Nakajima, D. Anazawa, H. A. Katori, and K. Prokes, J. Phys.: Condens. Matter **19**, 145244 (2007).
[12] S. Seki, Y. Yamasaki, Y. Shiomi, S. Iguchi, Y. Onose, and Y. Tokura, Phys. Rev. B **75**, 100403(R) (2007).
[13] N. Terada, T. Nakajima, S. Mitsuda, H. Kitazawa, K. Kaneko, and N. Metoki, Phys. Rev. B **78**, 014101 (2008).
[14] T. Nakajima, S. Mitsuda, S. Kanetsuki, K. Tanaka, K. Fujii, N. Terada, M. Soda, M. Matsuura, and K. Hirota, Phys. Rev. B **77**, 052401 (2008).
[15] T. Nakajima, S. Mitsuda, K. Takahashi, M. Yamano, K. Masuda, H. Yamazaki, K. Prokes, K. Kiefer, S. Gerischer, N. Terada, H. Kitazawa, M. Matsuda, K. Kakurai, H. Kimura, Y. Noda, M. Soda, M. Matsuura, and K. Hirota, Phys. Rev. B **79**, 214423 (2009).
[16] S. Seki, Y. Onose, and Y. Tokura, Phys. Rev. Lett. **101**, 067204 (2008).
[17] K. Kimura, H. Nakamura, K. Ohgushi, and T. Kimura, Phys. Rev. B **78**, 140401(R) (2008).
[18] M. Soda, K. Kimura, T. Kimura, M. Matsuura, and K. Hirota, J. Phys. Soc. Jpn. **78**, 124703 (2009).
[19] T. A. Kaplan and S. D. Mahanti, Phys. Rev. B **83**, 174432 (2011).
[20] M. Kenzelmann, G. Lawes, A. B. Harris, G. Gasparovic, C. Broholm, A. P. Ramirez, G. A. Jorge, M. Jaime, S. Park, Q. Huang, A. Ya. Shapiro, and L. A. Demianets, Phys. Rev. Lett. **98**, 267205 (2007).
[21] A. J. Hearmon, F. Fabrizi, L. C. Chapon, R. D. Johnson, D. Prabhakaran, S. V. Streltsov, P. J. Brown, and P. G. Radaelli, Phys. Rev. Lett. **108**, 237201 (2012).
[22] R. D. Johnson, S. Nair, L. C. Chapon, A. Bombardi, C. Vecchini, D. Prabhakaran, A. T. Boothroyd, and P. G. Radaelli, Phys. Rev. Lett. **107**, 137205 (2011).
[23] M. Tokunaga, M. Akaki, T. Ito, S. Miyahara, A. Miyake, H. Kuwahara, and N. Furukawa, Nat. Commun. **6**, 5878 (2016).
[24] N. Terada, D. D. Khalyavin, P. Manuel, Y. Tsujimoto, K. Knight, P. G. Radaelli, H. S. Suzuki, and H. Kitazawa, Phys. Rev. Lett. **109**, 097203 (2012).
[25] R. Seshadri, C. Felser, K. Thieme, and W. Tremel, Chem. Mater. **10**, 2189 (1998).
[26] W. C. Sheets, E. Mugnier, A. Barnabé, Y. J. Marks, and K. R. Poeppelmeier, Chem. Mater. **18**, 7 (2006).
[27] N. Terada, D. D. Khalyavin, P. Manuel, Y. Tsujimoto, and A. A. Belik, Phys. Rev. B **91**, 094434 (2015).
[28] See Supplemental Material at http://link.aps.org/supplemental/10.1103/PhysRevB.99.064402 for the crystallographic information files for $3R$-$AgFeO_2$ (113 K) and $2H$-$AgFeO_2$ (293 K) obtained by the single-crystal x-ray diffraction measurements.
[29] D. Pandey and P. Krishna, *Curr. Top. Mater. Sci.* 9, 415 (1982).
[30] L. C. Chapon, P. Manuel, P. G. Radaelli, C. Benson, L. Perrott, S. Ansell, N. J. Rhodes, D. Raspino, D. Duxbury, E. Spill, and J. Norris, Neutron News **22**, 22 (2011).
[31] N. Terada, D. D. Khalyavin, P. Manuel, Y. Tsujimoto, K. Knight, P. G. Radaelli, H. S. Suzuki, and H. Kitazawa, EPJ Web Conf. **40**, 15008 (2013).
[32] J. Rodriguez-Carvajal, Phys. B (Amsterdam, Neth.) **192**, 55 (1993).
[33] M. Mekata, N. Yaguchi, T. Takagi, T. Sugino, S. Mitsuda, H. Yoshizawa, N. Hosoito, and T. Shinjo, J. Phys. Soc. Jpn. **62**, 4474 (1993).
[34] S. Mitsuda, H. Yoshizawa, N. Yamaguchi, and M. Mekata, J. Phys. Soc. Jpn. **60**, 1885 (1991)
[35] S. Mitsuda, N. Kasahara, T. Uno, and M. Mase, J. Phys. Soc. Jpn. **67**, 4026 (1998).
[36] S. Mitsuda, M. Mase, K. Prokes, H. Kitazawa, and H. A. Katori, J. Phys. Soc. Jpn. **69**, 3513 (2000).
[37] N. Terada, Y. Narumi, Y. Sawai, K. Katsumata, U. Staub, Y. Tanaka, A. Kikkawa, T. Fukui, K. Kindo, T. Yamamoto, R. Kanmuri, M. Hagiwara, H. Toyokawa, T. Ishikawa, and H. Kitamura, Phys. Rev. B **75**, 224411 (2007).

[38] T. T. A. Lummen, C. Strohm, H. Rakoto, and P. H. M. van Loosdrecht, Phys. Rev. B **81**, 224420 (2010).
[39] N. Terada, S. Mitsuda, T. Fujii, K. Soejima, I. Doi, H. A. Katori, and Y. Noda, J. Phys. Soc. Jpn. **74**, 2604 (2005).
[40] B. J. Campbell, H. T. Stokes, D. E. Tanner, and D. M. Hatch, J. Appl. Crystallogr. **39**, 607 (2006).
[41] J. M. Perez-Mato, J. L. Ribeiro, V. Petricek, and M. I. Aroyo, J. Phys.: Condens. Matter **24**, 163201 (2012).
[42] S. Kimura, T. Fujita, N. Nishihagi, H. Yamaguchi, T. Kashiwagi, M. Hagiwara, N. Terada, Y. Sawai, and K. Kindo, Phys. Rev. B **84**, 104449 (2011).
[43] H. K. Zuo, L. R. Shi, Z. C. Xia, J. W. Huang, B. R. Chen, Z. Jin, M. Wei, Z. W. Ouyang, and G. Cheng, Chin. Phys. Lett. **32**, 047502 (2015).
[44] R. S. Fishman, Phys. Rev. Lett. **106**, 037206 (2011).
[45] J. P. Doumerc, A. Wichainchai, A. Ammar, M. Pouchard, and P. Hagenmuller, Mater. Res. Bull. **21**, 745 (1986).
[46] A. Vasiliev, O. Volkova, I. Presniakov, A. Baranov, G. Demazeau, J.-M. Broto, M. Millot, N. Leps. R. Klingeler, B. Büchner, M. B. Stone, and A. Zheludev, J. Phys.: Condens. Matter **22**, 016007 (2009).
[47] T. Nakajima, S. Mitsuda, S. Kanetsuki, M. Yamano, S. Iwamoto, Y. Yoshida, H. Mitamura, Y. Sawai, M. Tokunaga, K. Kindo, K. Prokes, and A. Podlesnyak, Phys. Rev. B **81**, 014422 (2010).
[48] T. Nakajima, A. Suno, S. Mitsuda, N. Terada, S. Kimura, K. Kaneko, and H. Yamauchi, Phys. Rev. B **84**, 184401 (2011).
[49] T. Nakajima, S. Mitsuda, J. T. Haraldsen, R. S. Fishman, T. Hong, N. Terada, and Y. Uwatoko, Phys. Rev. B **85**, 144405 (2012).
[50] K. Momma and F. Izumi, J. Appl. Crystallogr. **41**, 653 (2008).